Received: 1 May 2018 | Revised: 5 August 2018 | Accepted: 22 August 2018

DOI: 10.1002/cem.3081

RESEARCH ARTICLE

WILEY Journal of CHEMOMETRICS

A method for improvement of mass resolution and isotope accuracy for laser ablation time-of-flight mass spectrometers

Reto Wiesendanger[1,2] | Marek Tulej[1] | Valentine Grimaudo[3] | Alena Cedeño-López[3] | Rustam Lukmanov[1] | Andreas Riedo[4] | Peter Wurz[1]

[1]Space Research and Planetary Sciences, Physics Institute, University of Bern, Switzerland

[2]Microsystems for Space Technologies Laboratory, Ecole Polytechnique Fédérale, Lausanne, Switzerland

[3]Department of Chemistry and Biochemistry, Interfacial Electrochemistry Group, University of Bern, Switzerland

[4]Sackler Laboratory for Astrophysics, Leiden Observatory, Leiden University, Leiden, The Netherlands

Correspondence
Reto Wiesendanger, Space Research and Planetary Sciences, Physics Institute, University of Bern, 3012, Switzerland.
Email: reto.wiesendanger@space.unibe.ch

Funding information
Schweizerischer Nationalfonds zur Förderung der Wissenschaftlichen Forschung

Abstract

Accumulation of spectra is a common approach for improvement of the signal-to-noise ratio (SNR) in mass spectrometry. However, severe degradation of the overall spectrum can occur if some individual mass spectra, affected by peak broadening, are included in the accumulation process. In this contribution, we discuss potential sources and effects of spectral distortions by using examples from mass spectra acquired by our miniature laser ablation/ionisation time-of-flight mass spectrometer. We show how recent developments in acquisition systems enable to identify individual spectra subjected to peak broadening and present a filtering method capable of systematic and reproducible exclusion of such spectra from the accumulation process. We show that the method can be used on a wide range of materials and present a detailed case study performed on a trevorite mineral sample. Using this method, improvements of the isotope accuracy of Si, Ni, and Cr by factors between 1.6 and 7.7 were achieved. Finally, we discuss the limitations of the method and provide complementary analysis of other materials in the supplementary documents provided with this contribution.

KEYWORDS

filtering method, improvement of quantitative performance, isotope accuracy, laser ablation and ionisation time-of-flight mass spectrometry (LIMS-TOF), mass resolution

1 | INTRODUCTION

Since their development in the 1970s,[1] laser ablation and ionisation mass spectrometer (LIMS) instruments were used for the analysis of solid samples in combination with appropriate standard reference materials. In the early years of this century, the LIMS technique has been qualified as a semiquantitative method.[2-8] The quantitative performance is found to be limited, first, by the performance of the laser ion source[3,5,9] with its dependence on several laser parameters and, second, by the mass analyser with limited ion-optical performance. With the progress in laser technology, including the development of femtosecond laser sources, improvements of mass analyser design, and modelling tools, these fundamental limitations were substantially reduced during the last decade. The quantitative analysis of element and isotope abundances of various samples ranging from NIST standard materials to samples of rocks was recently demonstrated.[10,11] Even though these quantitative measurements are nowadays possible, their realisation can still be difficult,

because several sources of noise and spectral distortion effects can affect the mass spectra quality and limit the performance of an instrument. These limitations can be generally separated in two categories:

The first category involves all random noise sources that add to the measured spectra. To mitigate their influence, often hundreds to thousands of spectra are accumulated to enhance the signal-to-noise ratio (SNR). This improves the measurement accuracy and the ability to detect trace elements. Using this accumulation process, one achieves an improvement in accuracy of the element abundance and isotope ratio as well as detection limits of trace elements.[11,12]

The second category involves distortion effects that cannot be mitigated by purely statistical means. Phase correlated, nonrandom high-frequency noise belongs into this category. Techniques like smoothing, Fourier filtering, and wavelet filtering are commonly applied to reduce its influence.

The second category also includes signal ringing due to impedance mismatch in the signal transmission line and capture of high frequency electromagnetic radiation that are introduced into the signal path through inductive or capacitive coupling (cross-talk). Signal ringing is commonly reduced by using appropriate, impedance-matched signal transmission lines with a double or triple shielded to reduce signal distortions from external noise sources.

In this contribution, we treat high-amplitude, low-frequency spectral distortions that cannot be recovered by the techniques mentioned above. In particular, accumulation of a number of spectra can make the resulting mass spectrum worse instead of improving its SNR or mass resolution. Figure 1 illustrates the effects of spectral quality degradation after accumulation of 627 spectra. Panel A shows a well-resolved single spectrum, with peak widths at 10% over the baseline of approximately 50 nanoseconds. If only spectra of this quality would be accumulated, and assuming that peak shift has a minor influence (see Data S1), the overall spectrum shown in panel C should exhibit only mass peaks with widths in the range of approximately 50 nanoseconds. However, the overall spectrum was obtained by the inclusion of several spectra similar to the one shown in panel B. These spectra are of low resolution (peak widths at 10% over the baseline of several hundreds of ns), show peak intensities fluctuating from shot to shot, and suffer from distorted mass peak shapes. After accumulation of all 627 spectra, the distorted spectra deteriorate the baseline (panel C). Large sections of the mass range between m/q = 20 and 32 or 52 and 63 are not usable for conducting precise isotope analysis, and even identification of elements and their quantitative analysis can be very difficult because the widths of minor peaks become large and SNR is observed to decrease.

Other authors reported similar issues and mostly attributed the source of the distortions to a lack of shot-to-shot stability of the ablation laser.[13-15] In particular, when Q-switched lasers (eg, Nd:YAG laser operating in the ns pulse range) are used, the shot-to-shot fluctuations of the pulse are commonly in the range of a few percent, but values high as 40% were measured in our previous measurements.[4] If working close to the ablation threshold, such fluctuations can indeed have a strong impact on the ion production rates.[16]

The Ti:Sapphire laser system used in our set-up (operating with fs laser pulses) has a much better shot-to-shot pulse energy stability[9] of less than 6‰. This is achieved by controlling the laser's environment in terms of temperature, humidity, vibration, and air flow, a common approach to mitigate laser instabilities.

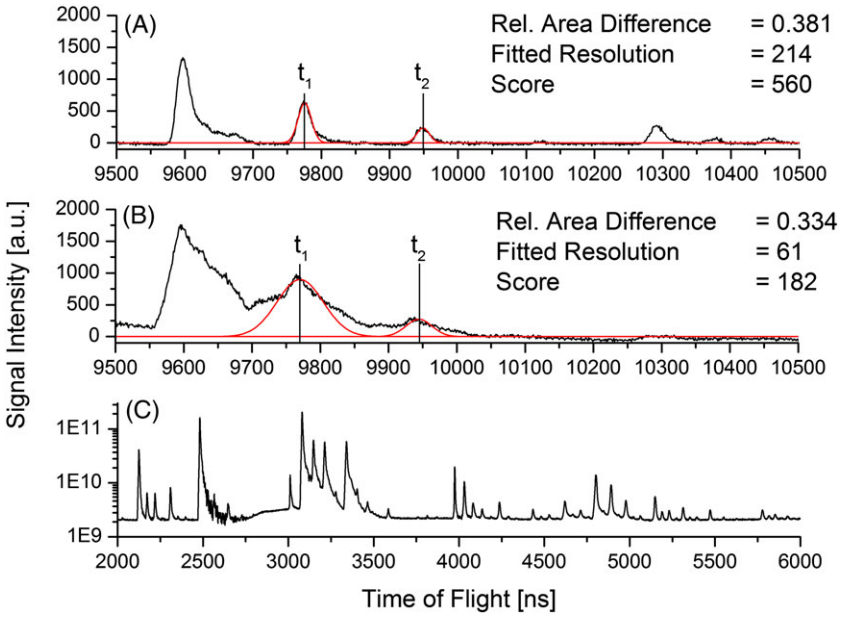

FIGURE 1 Mass spectrum of a sample of Trevorite mineral. A, Well-resolved spectrum before accumulation; B, spectrum showing excessive peak broadening before accumulation; C, accumulation of 627 spectra, including A and B. Red, fitted Gaussian peaks; see text for explanation of Rel. Area Difference, Fitted resolution

We can therefore exclude excessive fluctuations in the laser shot-to-shot stability as a source for the observed distortions and rather attribute their origin to non-linear behaviour of the ion yield during crater formation processes and on grain boundaries on heterogeneous or porous sample material.[16] A high ion yield then causes charging of the sample surface or space charge effects inside the ablated ion plume.[17,18] In some extreme cases, the resulting spatial and energy spread of the ablated plume may exceed the capabilities of energy and spatial focusing of the ion optical system, which results in mass spectra of low spectral resolution. Hence, the isolation of single spectra, affected by low-frequency high-amplitude distortions from the overall number of accumulated spectra, is of considerable interest for improving the SNR and mass resolution and thereby the quantitative performance. To the best of our knowledge, no method was presented so far to treat these problems.

One of the reasons of delay in development of relevant spectra treatment is that fast data acquisition systems became available only recently. In the past, the acquisition computer's bus and memory's limited capacities required to histogram data on the acquisition system prior to storage. This prevented the analysis of spectra acquired from single laser shots (or histograms of a few ten to hundred shots). Nowadays, fast data bus and large solid-state storage systems are readily available and allow to acquire spectra with frequencies of 1 kHz or larger. This opens the possibility of an individual assessment of each acquired spectrum.

The method for such an assessment must comply with a minimal set of requirements to guarantee quantitative results that can be used in a scientific context:

1. It must be reproducible.
2. It should not bias the result by introducing a priori knowledge.
3. For optimal usability, the process should also be highly automatized because a large amount of data needs to be processed.

2 | MATERIALS AND METHODS

2.1 | Evaluation of spectra

A method that complies with these requirements is to automatically analyse peak shapes and attribute a score (S) according to the spectral quality to each individual spectrum prior to the accumulation. The score is determined by comparing the measured mass peaks to a theoretical peak profile. In our method, the profile contains two neighbouring mass peaks, which allows to assess the separation of the peaks. This is of particular interest when accurate isotope determination is required. In the simplest case, the two neighbouring peaks can be perfectly described by composing two Gaussian curves. Although this model is an oversimplification in many cases, it turned out to work sufficiently well in our case.

For the theoretical peak profile, it is not sufficient to assume that the parameters of the Gauss distributions (standard deviation σ and amplitude A) are fixed, because the intensity of the acquired signal can vary over a wide range during a measurement campaign, regardless of the quality of the spectrum. Using fixed parameters would therefore lead to a rejection of many spectra, for the sole reason of not being close to the profile parameters set by the user. Thus, the theoretical profile needs to be determined for each spectrum individually.

A main advantage of the Gaussian distribution compared with other peak functions (eg, exponentially modified Gauss) for our application is that only two parameters, A and σ, need to be determined (Equation 1):

$$f(t) = \frac{A}{\sigma\sqrt{2\pi}} e^{\frac{-1}{2}\left(\frac{t-t_x}{\sigma}\right)^2}. \tag{1}$$

This accelerates the algorithm, makes the score attribution more robust, and simplifies the interpretation of results. Thus, considering two mass peaks in the analysis, only four parameters need to be found for each single measurement. A least-square algorithm that minimises the difference between the fitted curve and the measured data was implemented in MATLAB to obtain these parameters. The fitted curves for ^{56}Fe and ^{58}Ni are represented in red in Figure 1.

The difference between the theoretical peak profile and the measured data gives a direct measure for the quality of the spectrum, and minimal values could be used to select the best spectra. However, fluctuations in the peak intensities

in the individual mass spectra make it impossible to directly analyse the difference. Normalising this difference to the signal strength in the interval between the two mass peaks can provide a more reliable measure of the quality of the spectrum. This relative area difference is defined according to Equation 2:

$$\Delta_A = \frac{\sum_{t2}^{t1} |m(t) - g(t)|}{\sum_{t2}^{t1} m(t)}, \tag{2}$$

where $m(t)$ is the discrete measured signal value at time t (black line in Figure 1) and $g(t)$ is the fitted profile (red line), t_1 is the midpoint of the first fitted peak, and t_2 is the midpoint of the second fitted peak. The absolute of the difference is taken to avoid that random fluctuations around the theoretical profile compensate each other.

Because the peak fit algorithm can approximate broad peaks with broad, high σ-Gaussian distribution curves, the relative area difference alone is not a sufficient measure for the quality of a spectrum. Figure 1B shows an example for such a case: Despite the distortion, the relative area difference is lower than for the well-resolved spectrum in panel A. To cope with this effect, the mass resolution of the first fitted peak (Equation 3) is also taken into account for the calculation of the score. This allows to reject spectra with broad peaks efficiently.

$$R_1 = \frac{m}{\Delta m} = \frac{1}{2}\frac{t_1}{\Delta t_1} = \frac{1}{2}\frac{t_1}{2\sqrt{2\ \ln(2)}\sigma_1}. \tag{3}$$

Because the relative difference should be minimised and the resolution should be maximised, the score for a spectrum can be defined according to Equation 4:

$$S = \frac{R_1}{\Delta_A}. \tag{4}$$

If the distortion is so strong that a Gaussian cannot be fitted, a negative value is assigned to σ, leading to a negative score. Exclusion of spectra with a negative or low positive score increases therefore the quality of the spectrum.

2.2 | Samples

Because mineralogical studies are prioritised in our research group, we demonstrate the performance of the method on a mineral with known isotope composition. In this contribution, we used existing data acquired from the trevorite mineral[19] ($NiFe_2O_4$) to demonstrate the performance of our filtering method. During the trevorite measurement campaign, the mass spectra were taken at 10 different locations applying pulse energies close to 1 μJ/shot. On each measurement location, 230 to 630 individual spectra were acquired, each one containing an accumulation of 100 laser cycles. Figure 1 C depicts a typical mass spectrum acquired during this campaign.

Only the isotope ratios of the two main isotopes 58 and 60 were analysed because the SNR for the other isotopes 61, 62, and 63 was too low (<10-15 for the ^{62}Ni unfiltered spectra series) for a thorough analysis. Moreover, the isotope 64 is also subjected to isobaric interference with possible traces of Zn or Mg_2O; see Figure 3.

Because the measurement of the main element Mg can suffer from detector saturation effects, we have investigated the Si isotopes to study the performance of the method on major elements and the ^{52}Cr/^{53}Cr ratio as an additional minor element. Because of isobaric interference with ^{54}Fe, it was not possible to analyse the other ^{54}Cr isotope with sufficiently high accuracy.

Additional performance studies of the method on homogenous materials, such as NIST 981 Pb isotope standard and Yb- and Ge-doted laser fibres, can be found in Data S1.

2.3 | Determination of threshold score

The first step after taking the measurements is to find an optimal threshold score that guarantees good statistics while removing the largest possible number of spectra containing distortions from the overall mass spectrum. The distortions tend to broaden the mass peaks, especially at their base. The width of the base can therefore serve as a measure of the quality of the accumulated spectrum. For the determination of the optimal threshold, we have measured the full width at 10% of the maximum. To obtain the results shown in Figure 2, we have produced 13 accumulated spectra with

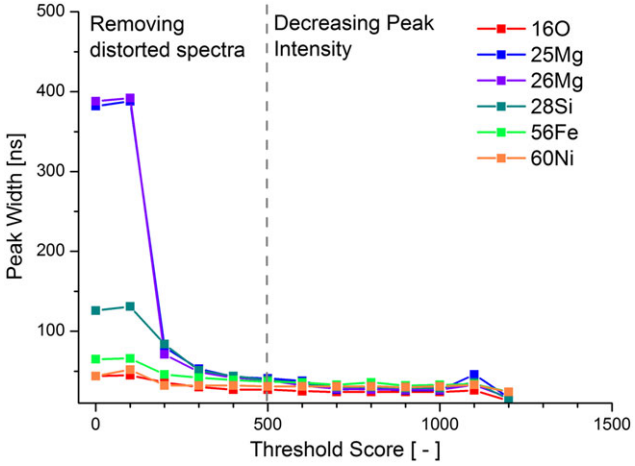

FIGURE 2 Determination of the threshold score (see text for explanation)

different threshold scores using the raw data obtained on one spot on the trevorite sample. Only spectra that were rated with a score above the threshold score were included in the overall accumulation.

We investigated the behaviour of major (O, Mg, and Si) and minor (Fe and Ni) elements. Both major and minor elements show the same trend. At low-scored peaks, the peak width at 10% is broad enough to overlap with several adjacent mass peaks, corresponding to a width of several hundreds of samples. When spectra with strong distortions (ie, low scores between 0 and 200) are removed, individual peaks become more distinct, and the measured peak width drops quickly. Above S = 200, the distortions affect the peaks more locally, and a gradual stabilisation towards a peak width of approximately 200 samples can be observed when approaching a score of S = 500. Above this limit, the peak width is observed to be relatively constant around approximately 50 nanoseconds close to the value expected from a single spectrum (Figure 1A). Further removal of single spectra does not increase the quality of the accumulation. However, the major peaks, especially Mg and Si, show much broader peak widths at low scores. This can be explained with the high ion flux of these elements, which can lead to an excessive peak broadening due to space charge effects. The initial peak broadening is less pronounced for peaks with only one isotope above the noise level such as O, or minor peaks such as Fe and Ni. Thus, the value of S = 500 is considered to be a threshold score that provides an optimal balance between the number of removed files and improvements of SNR due to sufficiently high number of accumulated spectra. Similar observations are made while analysing homogenous samples as demonstrated in Data S1 provided with this contribution.

Once a threshold is determined for one data set (a measurement location on the sample), it is then also applicable to data sets of any other measurements at other location, assuming that the same instrument settings are applied to acquire the spectra. We prove this by evaluating the performance of the method on 10 measurement locations on a trevorite sample, analysing the Ni isotope ratios.

3 | LIMS TOF INSTRUMENT

The measurements are conducted with our miniature laser mass spectrometer (LMS) composed of a grid-less reflectron-type TOF mass spectrometer and a femtosecond laser-ablation ion source and are described in full detail in our previous publications.[4,9,12,20,21] In this contribution, we only give a short overview of the system.

The compact instrument prototype (approximately 160 mm long and ∅60 mm) scheme is shown in Figure 3. The instrument was built for in situ analysis of planetary solids.[22] When placed on a planetary rover or a lander, the element and isotope analysis of planetary rocks and soils can be conducted with micrometre resolution. The measurements can be used to obtain information on mineralogical context, and element and isotope fractionation processes. These data can be used to determine times of formation of the planetary solids and provide insights into geological processes shaping planetary surface.[4,18,23,24] The mass spectrometric analyses can be also of primary importance in detection of bio-signatures.[21,23,25]

The instrument is operated in a vacuum chamber at pressures in the 10^{-8} mbar range. The investigated sample is positioned some hundreds of μm from the instrument's aperture, where the laser ($\lambda = 775$ nm, $\tau \sim 190$ fs, repetition rate ≤ 1 kHz, max pulse energy = 1 mJ/pulse) is focussed to a spot of 10 to 15 μm. Positively charged ions that are produced during the

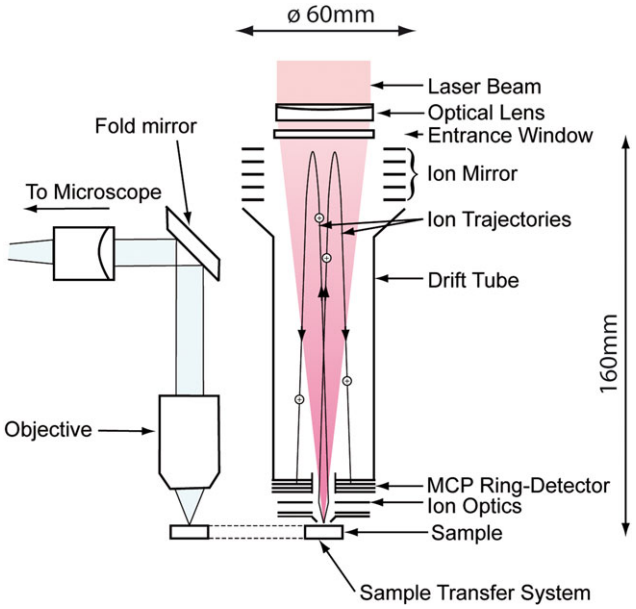

FIGURE 3 Schematic drawing of the laser mass spectrometer instrument including laser ablation and ionisation time-of-flight mass spectrometry and microscope system

laser ablation/ionisation are accelerated and confined into the field-free drift space through a series of electrodes. Subsequently, the beam is reflected and time-focussed on the detector by an ion mirror. The detector consists of two multichannel plates (MCP) in chevron configuration mounted on a microstrip five-ring anode plate with four output signal channels.[20] This architecture allows measurements with dynamic ranges of up to 10^8 and sensitivities below ppm levels.

Two 8-bit two-channel ADC cards with a sampling speed of 4 GS/s are used to acquire the spectra. A custom-made microscope next to the mass spectrometer allows to locate and sample features of interest in heterogeneous samples with μm accuracy.[21] The data analysis is performed using our in-house software[26] that uses the Simpson method for peak area determination.

3.1 | Determination of isotope ratios and relative accuracy

Before calculating the isotope ratios, the weak isobaric interference between the ^{58}Fe and ^{58}Ni isotopes must be resolved. Assuming terrestrial isotope ratios,[19,27] the abundance of ^{58}Fe can be estimated according to Equation 5:

$$A_{Fe}^{58} \sim \frac{0.00282}{0.99718} * \left(A_{Fe}^{54} + A_{Fe}^{56} + A_{Fe}^{57}\right). \tag{5}$$

This estimated value can then be subtracted from the peak area at m/q = 58 to obtain a corrected value for ^{58}Ni. After this correction, the isotope ratios can be calculated from the peak areas obtained from numerical Simpson integration.[26] The relative isotope accuracy is defined as

$$IA_R = \frac{C_{meas} - C_{ref}}{C_{ref}}, \tag{6}$$

where C_{meas} is the measured isotope ratio and C_{ref} is the isotope ratio in the standard.

4 | RESULTS AND DISCUSSIONS

The improvements to the derived relative isotope accuracy achieved by applying our spectrum-filtering algorithm become visible when analysing mass spectra affected by effects of spectral degradation. Figure 4, lower panel, shows the histogram of all calculated scores on one location on the sample obtained by analysing the ^{58}Ni and ^{60}Ni peaks. For 200 of the 238 spectra, the peak fitting was successful, resulting in a positive score. In 38 cases, the peak fit failed,

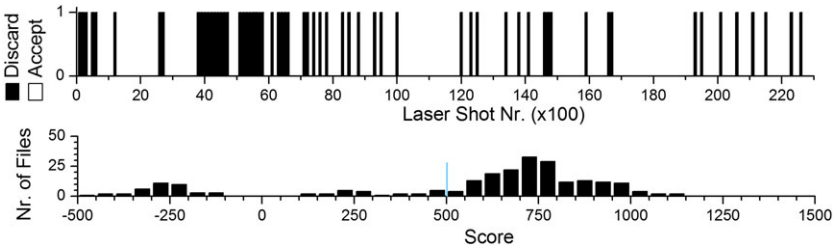

FIGURE 4 Accepted and discarded spectrum versus laser shot number (top panel); histogram of scores for 238 spectra (lower panel). The blue line indicates the threshold value determined above

and a negative score was attributed to these files. Figure 4, lower panel, also confirms that at the threshold score of 500, determined before, is also a suitable choice in terms of statistics because only a small part (26%) of the spectra will be removed.

Figure 4, upper panel, shows a typical distribution of the discarded files in the sequence of individual measurements. Many degraded spectra were recorded close to the surface (left side in Figure 4, upper panel). We attribute this effect to the initial crater formation process, occurring typically during the first 5000 to 10 000 laser shots.[16] Afterwards, the mass peak intensities and mass resolution stabilise, and only a few files have to be discarded in a random occurrence pattern. This threshold score guarantees a good averaging over the remaining measurement range once the crater is established.

We found that when other peak pairs, for example, ^{28}Si and ^{29}Si, are used for the determination of the score and the threshold score, similar results are obtained. A more detailed analysis of the dependencie of the score on the peak pair can be found in Data S1.

After removing spectra with a score lower than the threshold score and subsequent accumulation, the spectrum displayed in dark blue on Figure 5 is obtained. To facilitate a direct comparison, the original unfiltered spectrum is also shown in light blue. Some mass peaks that were difficult to recognise in the original spectrum such as ^{27}Al are now readily distinguishable from the neighbouring Si and Mg peaks. The same is true for the Cr and Fe isotopes that are sufficiently resolved to conduct the quantitative isotope analysis. After filtering, the peak width at 10% intensity decreases by factors of 2 to 8 (see Figure 2). This improves the detection of the peak area integration window and thereby the quantitative performance.

The isotope accuracies in 70 cases (seven isotope accuracies on 10 locations on the sample) were analysed, and the results are summarised in Figure 6. The light-blue squares represent the relative isotope accuracy before applying the filtering method, and the dark-blue circles represent the corresponding value after applying the filtering method. The error bars of the individual measurements are smaller than the marker size of the data points and are mainly due to the integration error of the Simpson method. The outlined squares and circles indicate the mean relative isotope accuracy. The error bars here represent the standard error of the mean, assuming a student distribution with a confidence interval of 0.95. The most important improvement was achieved on the ^{29}Si peak, where the relative isotope accuracy was improved by a factor of 7.7. For the other investigated relative isotope accuracies, an improvement factor in the range of 1.6 to 3.8 was achieved. All means of the measurements of the investigated isotopes improved due to the filtering, and for the individual measurements, only seven of the total 70 measured isotope ratios become worse after the filtering.

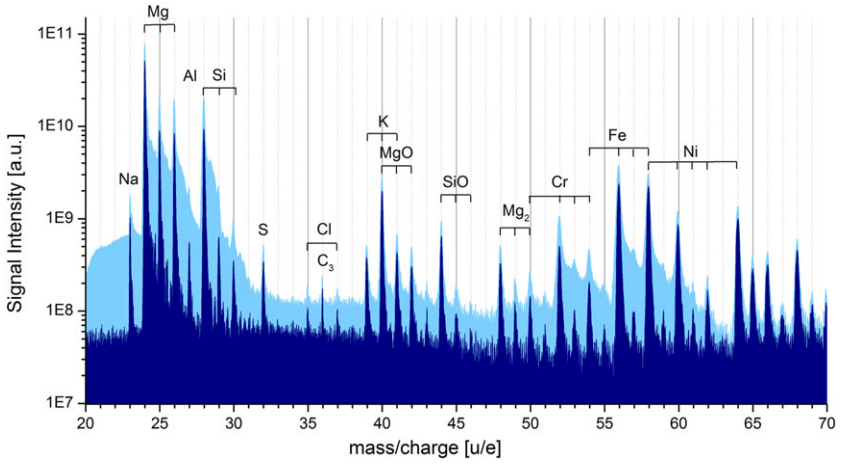

FIGURE 5 Original (238 spectra, light blue) and filtered accumulation (dark blue), no further (noise) filtering was applied

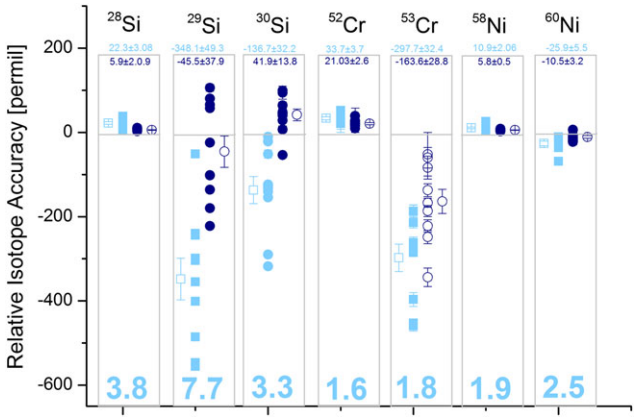

FIGURE 6 Relative isotope accuracies for the unfiltered spectrum (light blue) and the filtered spectrum (dark blue). Open and closed symbols give the individual measurements and the mean of the measurements, respectively. The numbers at the top of the boxes indicate the mean isotope accuracies and the standard error of the mean before and after the filtering process. The numbers at the bottom of the boxes correspond to the factor by which the isotope accuracy was improved

On three of the 10 locations, good results were achieved when only 26.9% to 57.5% of the files were retained. On the remaining locations, only 8% to 30.8% of the spectra were discarded, and the losses of measurements are therefore in a more acceptable range.

4.1 | Limitations

In some cases, the proposed filtering method does not recover a good quality spectrum, or the method needs to be applied with caution. Using some examples encountered during our studies, we present the limitations of the method in this section.

1. The method analyses and judges the shape of selected peaks regardless of their origin. The peaks under investigation could come from a specific isotope or any isobaric interference of several isotopes or clusters. If an isotope ratio is altered by a strong interference between elements and clusters, it is therefore unable to improve isotope ratios in such a case.
2. If a signal ringing is present in the acquired spectrum, the method presented in this contribution cannot recover spectral quality. Because this type of distortion is in phase in all the files, eliminating a part of the files does not reduce the relative amplitude of the distortion, and our method would not improve the result.
3. Sampling over the interface between two materials with strongly different ablation/ionisation efficiencies can mislead the filtering algorithm. Spectra are taken when sampling across the boundary will be different before and after the boundary because changing material composition, changing ablation parameters, and possible matrix effects. Thus, the algorithm can potentially fail to fit peaks if it is present only in one of the two materials. This would then lead to partial or complete removal of one of the materials from the spectrum. This risk can be mitigated by analysing the information displayed in Figure 6 and comparing the unfiltered spectrum to the filtered spectrum. Using depth profiling information, as presented in previous publications,[28,29] erroneous filtering and altering of spectra due to material transitions can be excluded with good confidence.

5 | CONCLUSION

In this contribution, we have shown that individual distorted mass spectra can reduce the quality of the accumulated mass spectra, even if only a small fraction of the accumulated spectra are actually affected. Using the simple and reproducible filtering process presented in this contribution, we were able to reliably remove the distorted spectra from the accumulation and improve both mass resolution and relative isotope accuracy. After the filtering process, clearly distinct peaks can be identified in previously unresolved portions of the mass spectrum. The isotope accuracies derived

from the filtered spectrum were improved by factors of 1.6 to 7.7 for the investigated cases. We discussed limitations process and show examples where it has to be applied with caution.

ACKNOWLEDGEMENTS

We gratefully acknowledge the financial support of the Swiss National Science Foundation and H. Shea, Microsystems for Space Technologies Laboratory, Ecole Polytechnique Férérale Lausanne, Switzerland, for his support. This work was funded by Schweizerischer Nationalfonds zur Förderung der Wissenschaftlichen Forschung.

ORCID

Reto Wiesendanger http://orcid.org/0000-0001-7127-0516
Andreas Riedo http://orcid.org/0000-0001-9007-5791

REFERENCES

1. Hercules DM. Laser microprobe mass-spectrometry—the past, present, and future. *Microchem J*. 1988;38(1):3-23.
2. Riedo A, Grimaudo V, Moreno-Garcia P, et al. Laser ablation/ionisation mass spectrometry: sensitive and quantitative chemical depth profiling of solid materials. *Chimia*. 2016;70(4):268-273.
3. Zhang BC, He MH, Hang W, Huang BL. Minimizing matrix effect by femtosecond laser ablation and ionization in elemental determination. *Anal Chem*. 2013;85(9):4507-4511.
4. Riedo A, Bieler A, Neuland M, Tulej M, Wurz P. Performance evaluation of a miniature laser ablation time-of-flight mass spectrometer designed for in situ investigations in planetary space research. *J Mass Spectrom*. 2013;48(1):1-15.
5. Zhang SD, He MH, Yin ZB, Zhu EY, Hang W, Huang BL. Elemental fractionation and matrix effects in laser sampling based spectrometry. *J Anal Atom Spectrom*. 2016;31(2):358-382.
6. Huang RF, Yu Q, Li LF, et al. High irradiance laser ionization orthogonal time-of-flight mass spectrometry: a versatile tool for solid analysis. *Mass Spectrom Rev*. 2011;30(6):1256-1268.
7. Green T, Kuznetsov I, Willingham D, et al. Characterization of extreme ultraviolet laser ablation mass spectrometry for actinide trace analysis and nanoscale isotopic imaging. *J Anal Atom Spectrom*. 2017;32(6):1092-1100.
8. Ma Z, Thompson RN, Lykke KR, Pellin MJ, Davis AM. New instrument for microbeam analysis incorporating submicron imaging and resonance ionization mass-spectrometry. *Rev Sci Instrum*. 1995;66(5):3168-3176.
9. Riedo A, Neuland M, Meyer S, Tulej M, Wurz P. Coupling of LMS with a fs-laser ablation ion source: elemental and isotope composition measurements. *J Anal Atom Spectrom*. 2013;28(8):1256-1269.
10. Neuland MB, Grimaudo V, Mezger K, et al. Quantitative measurement of the chemical composition of geological standards with a miniature laser ablation/ionization mass spectrometer designed for in situ application in space research. *Meas Sci Technol*. 2016;27(3):035904.
11. Riedo A, Meyer S, Heredia B, et al. Highly accurate isotope composition measurements by a miniature laser ablation mass spectrometer designed for in situ investigations on planetary surfaces. *Planet Space Sci*. 2013;87:1-13.
12. Wiesendanger R, Tulej M, Riedo A, Frey S, Shea H, Wurz P. Improved detection sensitivity for heavy trace elements using a miniature laser ablation ionisation mass spectrometer. *J Anal Atom Spectrom*. 2017;32(11):2182-2188.
13. Anderson FS, Levine J, Whitaker TJ. Dating the Martian meteorite Zagami by the Rb-87-Sr-87 isochron method with a prototype in situ resonance ionization mass spectrometer. *Rapid Commun Mass Sp*. 2015;29(2):191-204.
14. Wurz P, Lykke KR, Pellin MJ, Gruen DM, Parker DH. Characterization of fullerenes by laser-based mass-spectrometry. *Vacuum*. 1992;43(5-7):381-385.
15. Anderson FS, Levine J, Whitaker TJ. Rb-Sr resonance ionization geochronology of the Duluth gabbro: a proof of concept for in situ dating on the moon. *Rapid Commun Mass Sp*. 2015;29(16):1457-1464.
16. Grimaudo V, Moreno-Garcia P, Lopez AC, et al. Combining anisotropic etching and PDMS casting for three-dimensional analysis of laser ablation processes. *Anal Chem*. 2018;90(4):2692-2700.
17. Brinckerhoff WB, Managadze GG, McEntire RW, Cheng AF, Green WJ. Laser time-of-flight mass spectrometry for space. *Rev Sci Instrum*. 2000;71(2):536-545.
18. Tulej M, Iakovleva M, Leya I, Wurz P. A miniature mass analyser for in-situ elemental analysis of planetary material-performance studies. *Anal Bioanal Chem*. 2011;399(6):2185-2200.
19. Gueguen B, Rouxel O, Ponzevera E, Bekker A, Fouquet Y. Nickel isotope variations in terrestrial silicate rocks and geological reference materials measured by MC-ICP-MS. *Geostand Geoanal Res*. 2013;37(3):297-317.

20. Riedo A, Tulej M, Rohner U, Wurz P. High-speed microstrip multi-anode multichannel plate detector system. *Rev Sci Instrum*. 2017, *[subm.]*;88(4):045114.

21. Wiesendanger R, Wacey D, Tulej M, et al. Chemical and optical identification of micrometre sized 1.9 billion-year-old fossils with a miniature LIMS system combined with an optical microscope. *Astrobiology*. 2018;18(8):1071-1080. https://doi.org/10.1089/ast.2017.1780

22. Rohner U, Whitby JA, Wurz P. A miniature laser ablation time-of-flight mass spectrometer for in situ planetary exploration. *Meas Sci Technol*. 2003;14(12):2159-2164.

23. Managadze GG, Wurz P, Sagdeev RZ, et al. Study of the main geochemical characteristics of Phobos' regolith using laser time-of-flight mass spectrometry. *Solar Syst Res*+. 2010;44(5):376-384.

24. Li X, Brinckerhoff WB, Managadze GG, Pugel DE, Corrigan CM, Doty JH. Laser ablation mass spectrometer (LAMS) as a standoff analyzer in space missions for airless bodies. *Int J Mass Spectrom*. 2012;323:63-67.

25. Tulej M, Neubeck A, Ivarsson M, et al. Chemical composition of micrometer-sized filaments in an aragonite host by a miniature laser ablation/ionization mass spectrometer. *Astrobiology*. 2015;15(8):669-682.

26. Meyer S, Riedo A, Neuland MB, Tulej M, Wurz P. Fully automatic and precise data analysis developed for time-of-flight mass spectrometry. *J Mass Spectrom*. 2017;52(9):580-590.

27. Becker JS. *Inorganic Mass Spectrometry Principles and Applications*. Chichester: John Wiley; 2007 p Online-Ressource.

28. Grimaudo V, Moreno-Garcia P, Riedo A, et al. Toward three-dimensional chemical imaging of ternary cu-Sn-Pb alloys using femtosecond laser ablation/ionization mass spectrometry. *Anal Chem*. 2017;89(3):1632-1641.

29. Grimaudo V, Moreno-Garcia P, Riedo A, et al. High-resolution chemical depth profiling of solid material using a miniature laser ablation/ionization mass spectrometer. *Anal Chem*. 2015;87(4):2037-2041.

SUPPORTING INFORMATION

Additional supporting information may be found online in the Supporting Information section at the end of the article.

How to cite this article: Wiesendanger R, Tulej M, Grimaudo V, et al. A method for improvement of mass resolution and isotope accuracy for laser ablation time-of-flight mass spectrometers. *Journal of Chemometrics*. 2018;e3081. https://doi.org/10.1002/cem.3081